https://doi.org/10.15407/ujpe71.4.321

T. GAVRILKO,[1,2] T. KHALYAVKA,[3,4] J.-C. GRIVEL,[3] YE. MANUILOV,[1]
V. SHYMANOVSKA,[1] M. CHAIKA,[2] M. DROZD[2]

[1] Institute of Physics of the Nat. Acad. of Sci. of Ukraine
(46, Nauky Ave., 03028 Kyiv, Ukraine)
[2] Institute of Low Temperature and Structure Research, Polish Academy of Sciences
(Ul. Okólna 2, 50-422 Wrocław, Poland; e-mail: gavrilko@gmail.com)
[3] Department of Energy Conversion and Storage, Technical University of Denmark
(Kongens Lyngby, 2800 Denmark)
[4] Institute for Sorption and Problems of Endoecology of the Nat. Acad. of Sci. of Ukraine
(13, Oleg Mudrak Str., 03164, Kyiv, Ukraine)

OPTICAL AND PHOTOLUMINESCENCE PROPERTIES OF RARE EARTH IONS-DOPED ANATASE/BROOKITE DUAL-PHASE TiO_2

For the first time, optical absorption and luminescent properties of nanostructured dual-phase anatase-brookite (A/B) TiO_2 doped with Sm^{3+}, Gd^{3+}, Tb^{3+}, Tm^{3+} and Yb^{3+} rear earth (RE) ions are reported. The RE-doped TiO_2 particles had a spherical shape with a typical size of 10–25 μm in diameter and consisted of grown together nanocrystallite aggregates of 5–8 nm. SEM/EDS analysis confirmed successful incorporation of RE-dopants onto the surface of the TiO_2 particles. With FTIR spectroscopy, a formation of RE–Ti–O and RE–OH bonds near the surface defect states was found. UV-Vis-NIR diffuse reflectance spectra exhibited a blue shift of the TiO_2 main absorption band maximum for Gd^{3+} dopant and a red shift of the absorption edge for Yb^{3+}. Several characteristic NIR absorption bands of RE ions were also detected for Sm^{3+}-, Tm^{3+}- and Yb^{3+}-doped TiO_2, assigned to their 4f-4f transitions, while Gd^{3+}- and Tb^{3+}-doped samples show no absorption in this region. The calculated band gap energies (E_g) of RE-doped TiO_2 were 3.02, 2.97, 2.93, 2.92, 2.88 and 2.91 eV, for undoped and doped with Sm^{3+}, Tm^{3+}, Tb^{3+}, Yb^{3+}, and Gd^{3+} samples, respectively. It was shown that under excitation of A/B TiO_2 nanocrystals above the TiO_2 band gap energy, the particles exhibited characteristic luminescence corresponding to 4f–4f transitions of RE^{3+} ions. It was explained that in RE-doped A/B dual-phase TiO_2 nanostructures, the regions at A/B junctions or grain boundaries of TiO_2 nanocrystals can easily accommodate RE^{3+} ions and provide for efficient energy transfer from TiO_2 to RE^{3+} ions under appropriate alignment of excited state energy levels of the dopant in TiO_2 band gap. Such energy transfer was observed only in samples doped with Sm^{3+}, Tb^{3+}, and Tm^{3+}, while no emission was observed for Yb^{3+}- and Gd^{3+}-doped TiO_2 due to the higher energy of their excited states. RE-doped A/B dual-phase TiO_2 nanostructures may find potential applications in various optical and engineering fields, such as LED, optic systems, communication devices, and heterogeneous photocatalysis.

Keywords: TiO_2, nanocrystals, rare earth, UV-Vis-NIR absorption, luminescence, energy transfer.

1. Introduction

The rare earth (RE) elements with atomic numbers from 57 to 71 in periodic table (from lanthanum La to lutetium Lu) are nowadays extensively used in modern technology as an integral part of advanced electronic devices, LEDs and fiber optic applications, power generation technologies and military products [1]. Due to the unique set of energy levels

Citation: Gavrilko T., Khalyavka T., Grivel J.-C., Manuilov Ye., Shymanovska V., Chaika M., Drozd M. Optical and photoluminescence properties of rare earth ions-doped anatase/brookite dual-phase TiO_2. *Ukr. J. Phys.* **71**, No. 4, 321 (2026). https://doi.org/10.15407/ujpe71.4.321.

of incompletely occupied $5d$ or $4f$ orbitals, systems based on RE ions generally exhibit intriguing spectroscopic properties, such as bright luminescence with sharp narrow emission bands in the UV-Vis and NIR ranges with a large number of allowed transitions, and long lifetimes [2, 3]. However, due to parity selection rule, direct excitation of the f–f transitions of the RE ions is forbidden. To become allowable, these "dark" transitions require symmetry breaking, such as electron-phonon interactions or external field effects. Recently, to overcome the intrinsic absorption limitations, the use of transition metal oxide host materials was proposed to excite the RE ions and significantly enhance their emission intensity [4–6] via the so-called "antenna effect" by their encapsulation in an inorganic host where transition metal ions of the host absorb light and then transfer energy to the RE ions.

As inorganic oxide hosts, ZnO [7], SnO_2 [8] and TiO_2 [9–12] are generally selected as the best candidates due to their thermal and chemical stability and good mechanical properties. The developed RE-doped systems mostly include thin films [13, 14]. The authors of [15, 16] demonstrated the intense emission from Eu^{+3} ions incorporated into spherical TiO_2 nanoparticles, which was explained by the energy transfer from the TiO_2 to Eu^{+3} ions. It was shown in that in spherical core-shell Eu-doped TiO_2 nanoparticles, due to the uniform distribution of Eu^{3+} ions inside the amorphous phase TiO_2, the undesired Eu^{3+} clustering is significantly suppressed, and characteristic visible emission from Eu^{3+}ions was observed under UV-excitation, which was explained by energy transfer between Ti^{3+} and Eu^{3+} ions [6]. However, in most cases, the RE dopants were mostly adsorbed on the oxide nanoparticle surface and so the only very weak luminescence of RE ions could be seen under their direct excitation. Therefore, special effort have to be made to prevent RE-RE aggregation in oxide matrices that causes concentration quenching of RE emission. In our recent papers [17, 18] we proposed to employ the anatase-brookite (A/B) dual-phase TiO_2 nanostructured material as a host for trivalent RE ions. It was shown that with simple synthesis procedure, the RE ions can be incorporated into the TiO_2 framework which resulted in nanocrystalline material with high surface area, small crystallite size, abundant dual-phase junctions and potential photocatalytic applications. However, general photophysical properties of these materials were still not studied in detail.

In continuation of these studies, in this work we focused on the effect of rare-earth doping on the optical and luminescence properties of nanocrystalline anatase/brookite (A/B) dual-phase TiO_2 doped with trivalent Sm, Gd, Tb, Tm and Yb ions. It is our aim to elucidate the mechanism of the energy transfer in these systems, which have never been studied before.

2. Experimental

2.1. Samples preparation and morphology characterization

For the research, powdered nanocrystalline anatase/brookite (A/B) dual-phase TiO_2 was used which consisted of spherical particles with a specific surface area of 165 m^2/g. The volume fractions of anatase and brookite in the unmodified A/B sample were 94 and 6%, and the mean crystallite sizes were about 9 and 8 nm respectively. Dual-phase A/B TiO_2 particles doped with 2 wt.% of Sm^{3+}, Gd^{3+}, Tb^{3+}, Tm^{3+} and Yb^{3+} rare earth (RE) ions were synthesized according to [17] and denoted as Sm-T, Gd-T, Tb-T, Tm-T and Yb-T, respectively. The prepared particles were of a spherical shape with a typical size of 10–25 μm in diameter and consisted of grown together nanocrystallite aggregates of 5–8 nm. The dual-phase A/B structure of RE–TiO_2 has been confirmed by X-ray phase and TEM analyses [17]. No peaks from any RE compound and no shift of the anatase peaks were detected after doping indicating that RE^{3+} ions do not occupy the Ti sites in the TiO_2 crystal lattice. It worth mentioning that generally, incorporation of RE into the TiO_2 crystal structure is difficult because of mismatch of the ionic radii (0.0745–0.1045 nm compared with 0.068 nm for Ti^{4+}), and therefore, the RE ions are rather accommodated near lattice voids or accumulated at grain boundaries, forming RE oxides. The high content of RE^{3+} dopant ions located on the surface of the RE-TiO_2 nanoparticles was confirmed by energy dispersive X-ray spectroscopy (EDX) measurements (Fig. 1).

2.2. Samples characterization methods

FT-IR absorption spectra were taken at room temperature with a Bruker IFS-88 spectrometer in the MIR (380–4000 cm^{-1}) and FIR (80–550 cm^{-1}) spectral ranges. Each spectrum was accumulated out

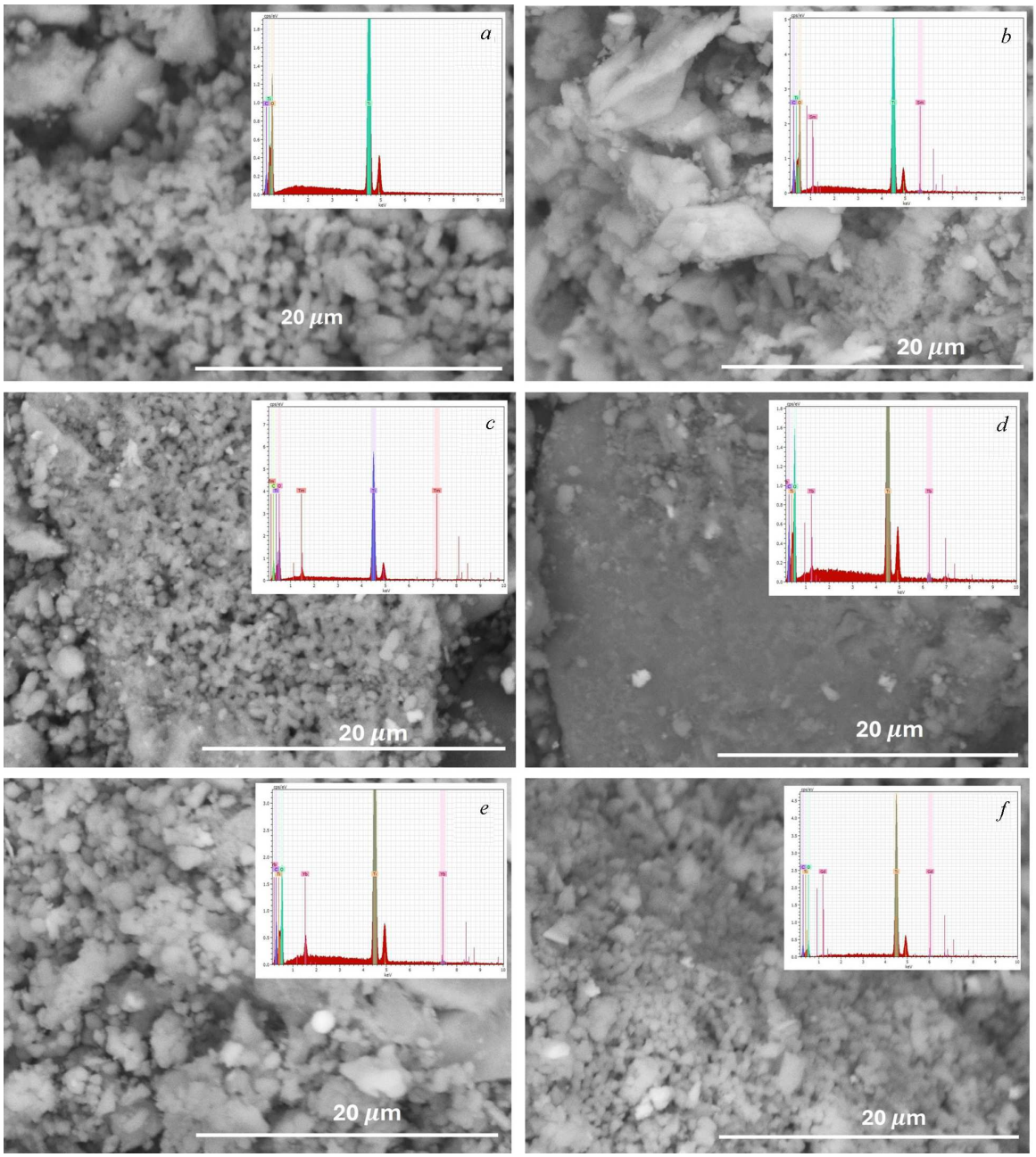

Fig. 1. SEM images and EDX spectra of the powders: TiO_2 (*a*), Sm-T (*b*), Tm-T (*c*), Tb-T (*d*), Yb-T (*e*), Gd-T (*f*)

of 64 scans with a resolution of 4 cm^{-1}. Samples for MIR spectra measurements were prepared using the KBr pellets technique, while those for FIR spectra measurements were mulled with Nujol and sandwiched between two Mylar windows. OriginPro 8.1 and Grams^{TM} spectroscopy software packages were applied for spectra processing (baseline correction and band shape deconvolution). UV-Vis-NIR absorption spectra of the samples were measured with a Cary Varian 5000 UV-Vis-NIR spectrometer, equipped with a diffuse reflectance accessory (UV-Vis-NIR Praying Mantis), two detectors – a photo-

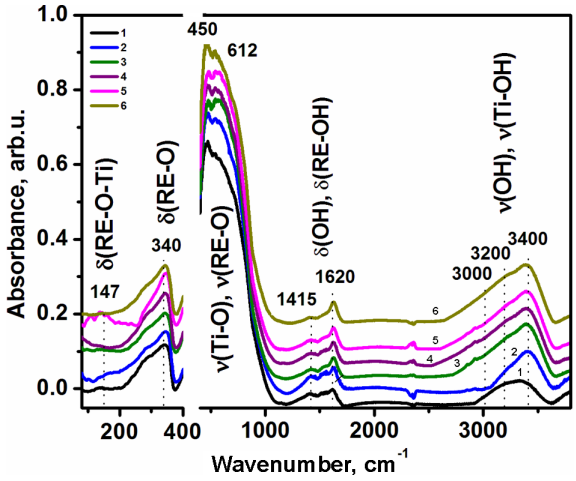

Fig. 2. Normalized FT-IR absorption spectra of the samples: TiO_2 (*1*), Sm-T (*2*), Tm-T (*3*), Tb-T (*4*), Yb-T (*5*), Gd-T (*6*)

multiplier in the UV-Vis spectral range (200–850 nm) and a PbSmart detector in the NIR range (850–2650 nm), and two light sources, tungsten halogen lamp in visible (340–2650 nm) and deuterium arc in UV (190–340 nm) spectral ranges. The resolution was 1 and 4 nm in the UV-Vis and NIR ranges respectively. The PL emission and excitation spectra were recorded with an Edinburgh Instruments FLS980 fluorescence spectrometer equipped with two detectors in the visible (Hamamatsu, R928P, 400–700 nm) and the NIR (Hamamatsu, R5509-72, 900–1600 nm) regions. A 266 nm diode laser (60 mW) was used as the excitation source. The emission spectra were collected at an emission slit width of 1.5 nm, which provided the spectral resolution of approximately 1 nm. Due to the low emission intensity, the background emission from the substrate table and the reflected laser half-energy excitation beam are visible on the collected emission spectra.

3. Results and Discussion

3.1. FTIR spectroscopy

FTIR spectroscopy measurements (Fig. 2) were used to confirm the presence of RE elements in RE-doped A/B dual-phase TiO_2. Our main purpose was to determine the additional bands or changes in the spectral parameters of the existing absorption bands that may be related to possible formation of RE–OH, RE–O or RE–O–Ti bonds after doping (Fig. 2). It can be seen from the Fig. 2, that FTIR spectrum of undoped A/B dual-phase TiO_2 clearly shows three main bands. The first broad band centred at 3400 cm^{-1} corresponds to stretching vibrations of hydrogen-bonded O–H groups of water molecules adsorbed on TiO_2 particles surface. Compared to single phase anatase, this band has an asymmetric shape with a shoulder at about 3000 cm^{-1} extended to lower frequencies. This observation indicates the existence of various OH groups in the A/B TiO_2 nanostructure, which are bound to TiO_2 particles with different hydrogen-bonding strengths [19] (Fig. 2), where the low-frequency shoulder corresponds to the most strongly hydrogen bonded water molecules possibly accommodated at A/B TiO_2 junctions or RE–Ti–OH groups related to different defect states. The second major absorption band is observed around 1630 cm^{-1} corresponding to OH bending vibrations of water. Here, the shoulders at 1540 and 1415 cm^{-1} have been attributed to bending modes of surface OH species at the TiO_2 A/B interface [20] or to Ti–O–H deformation vibrations. The fundamental vibrations of A/B TiO_2 nanocrystals appear in the IR-spectra as very strong broad bands, which originate from Ti–O (612 cm^{-1}) and Ti–O–Ti stretching vibrations (450 cm^{-1}) and are shifted to low frequencies compared to single-phase anatase [21] (by about 100 cm^{-1} for ν(Ti–O)) due to contribution of intrinsic lattice vibrations of brookite phase [22, 23]. Bending Ti–O–Ti vibrations are observed in far-IR spectral range at about 340 and 147 cm^{-1} (Fig. 2).

In the FTIR spectra of RE-doped A/B TiO_2, the absorption band of Ti–O stretching vibrations is slightly shifted towards lower frequencies. This behaviour could be attributed to the formation of weaker Ti–O–RE bonds. Analysis of the OH stretching region shows a decrease in the intensity of the low-frequency shoulder and an insignificant intensity redistribution between different components of the major absorption band indicating changes in surface-adsorbed water and hydroxyl groups on TiO_2 surface after RE-doping. The spectral region above the own absorption of TiO_2 nanocrystals is less affected by doping, however, here the peaks associated with surface hydration processes on the RE–TiO_2 nanoparticle surface are clearly seen (bands associated with deformation vibrations of surface OH groups at 1620 cm^{-1}, local defects at ~1540 cm^{-1} and RE–OH bonds of different dopants at about 1415 and below 1300 cm^{-1}). The far-IR spectra of RE-

doped TiO_2 (Fig. 2) are complex and vary for each specific dopant with an obvious low-frequency shift that is assigned to contribution from characteristic RE–O vibrational modes due to introduction of heavy lanthanide ions.

3.2. UV-Vis-NIR absorption

To study the optical absorption properties of RE-modified TiO_2 nanopowders, the UV-Vis-NIR diffuse reflectance spectra were investigated in the range of 300–2400 nm. Fig. 3 shows the absorption spectra of both undoped and RE-doped TiO_2 in UV–Vis spectral range (300–900 nm).

For all the samples, superior absorption in the region of 200–400 nm is observed with two maxima below 350 nm at 310 and 250 nm which is due to intrinsic absorption of anatase and brookite TiO_2, with band gap energies of about 3.6 eV and 3.4 eV, respectively. The position of the absorption maximum of both undoped and RE-doped A/B dual-phase TiO_2 is blue-shifted with respect to single-phase anatase (382 nm). This absorption is usually associated with the electronic transitions of $2p$ electron of oxygen from the valence band to the Ti $3d$ level in conduction band of TiO_2 [24]. RE-doping does not significantly affect the position of the absorption band maximum for Sm-, Tm-, Tb-, and Yb-TiO_2, which is blue shifted by ∼50 nm only for Gd dopant. At the same time, the red shift of the absorption band edge upon RE doping is registered for Yb-T only.

Using the Kubelka–Munk function $F(R_\infty)$ (Eq. 1), we estimated the band-gap energy of RE-doped TiO_2

$$F(R_\infty) = \frac{(1-R_\infty)^2}{2R_\infty} = \frac{K}{S}, \qquad (1)$$

where $F(R_\infty$ is the Kubelka–Munk function, K is the absorption coefficient, S is the scattering coefficient, $h\nu$ is the photon energy, and λ denotes the wavelength employed.

The optical band-gap energy E_g can be obtained from each UV-vis absorption spectrum using the Tauc's equation (Eq. 2)

$$[F(R_\infty)\, h\nu]^n = C(h\nu - E_g). \qquad (2)$$

In this case, C is a constant, n equals to 1/2 for indirect allowed, 3/2 for direct forbidden, 2 for direct allowed, and 3 for indirect forbidden transitions

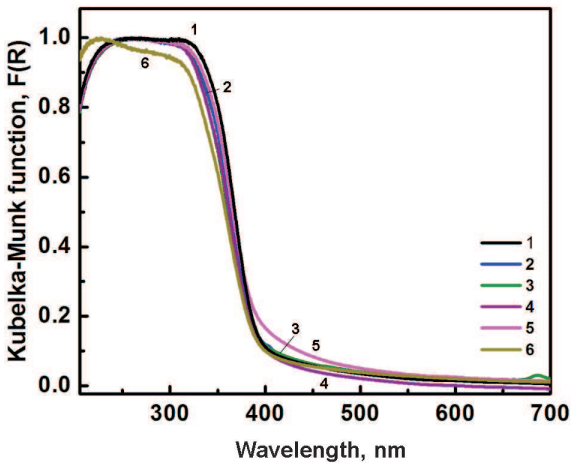

a

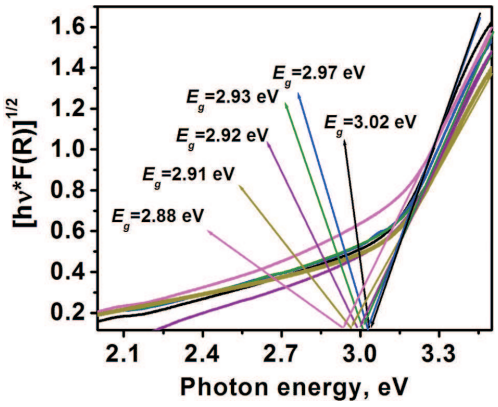

b

Fig. 3. UV-vis absorption spectra (*a*), and the Tauc's plots $F(R)^{1/2}$ versus photon energy, where $F(R)$ is the Kubelka–Munk function for (*b*): TiO_2 (*1*), Sm-T (*2*), Tm-T (*3*), Tb-T (*4*), Yb-T (*5*), Gd-T (*6*)

[25]. The band gap energy of the A/B dual-phase RE-TiO_2 was estimated for allowed indirect transition with $n = 1/2$.

The band gap value was estimated by linearly fitting the plot $(h\nu \cdot F(R\infty))^n$ vs $h\nu$ to intersection with the photon energy axis (Fig. 3, *b*). The obtained Eg values for undoped and RE-doped A/B dual-phase TiO_2 are around 3 eV making up 3.02, 2.97, 2.93, 2.92, 2.88 and 2.91 eV, for samples doped with Sm^{3+}, Tm^{3+}, Tb^{3+}, Yb^{3+}, and Gd^{3+}, respectively. The obtained E_g values appeared gradually decreasing from middle- (Sm, Tb, Gd) to heavy-RE (Tm, Yb) dopants. Such band gap values suggest that under irradiation with wavelength of 266 nm (∼4.7 eV) the electron-hole recombination will occur due to a di-

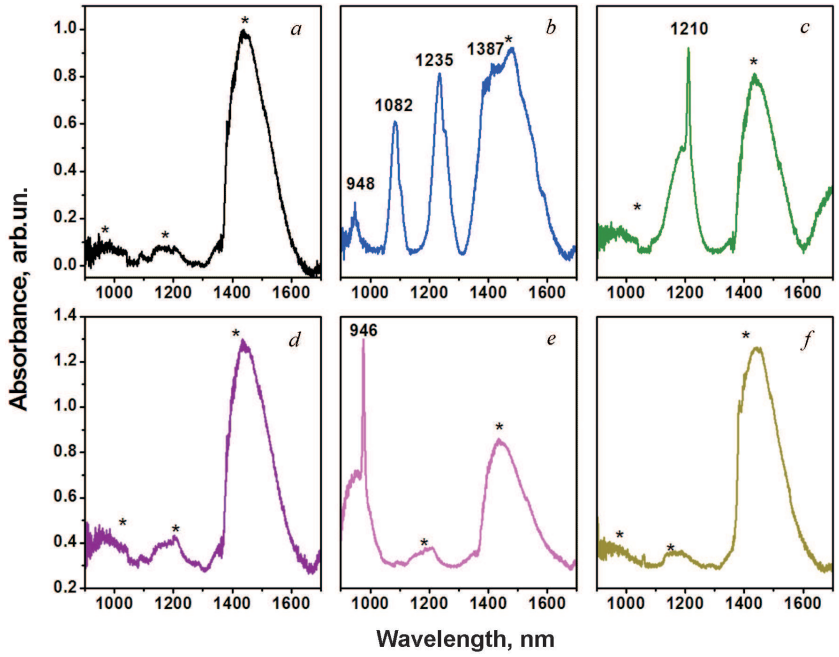

Fig. 4. Normalized (in relation to the most intense band in the range) NIR absorption spectra of RE-doped TiO_2 powders: TiO_2 (*a*), Sm-T (*b*), Tm-T (*c*), Tb-T (*d*), Yb-T (*e*), Gd-T (*f*). Asterisks indicate the bands corresponding to the absorption of matrix and water molecules

rect transition from the conduction to the valence band, emitting photons with the energy close to E_g (∼410 nm), which can be further transferred to the energy levels of RE ions via shallow defect states near the absorption edge.

When excited to these low energy levels, RE^{3+} ions can show near-infrared luminescence or be engaged in up-conversion processes [5]. However, we did not register directly any NIR emission intensity from RE-TiO_2 probably due to low detector sensitivity.

Also, a significant NIR absorption (800–2000 nm) was observed for RE-doped TiO_2 materials showing clear spectral features arising from $4f \rightarrow 4f$ electronic transitions of the RE ions [26] (Fig. 4) which confirms the presence of RE energy levels in the TiO_2 band gap. The major absorption bands are determined for Sm-doped TiO_2 at 948, 1082, 1235 and 1387 nm related to $^6H_{5/2} \rightarrow {}^6F_{11/2}$, $^6H_{5/2} \rightarrow {}^6F_{9/2}$, $^6H_{5/2} \rightarrow {}^6F_{7/2}$ and $^6H_{5/2} \rightarrow {}^6F_{5/2}$, electronic transitions in Sm^{3+} respectively [27].

The absorption spectrum of Tm-T shows sharp band at 1210 nm attributed to the $^3H_6 \rightarrow {}^3H_5$ electronic transition of Tm^{3+} ions [28]. While Yb-T shows a strong Yb^{3+} absorption peak at 946 nm, Gd^{3+} and Tb^{3+} lack significant features in this range due to their $4f$–$5d$ transitions occurring below 400 nm. Such spectral disparities between middle- and heavy-RE ions likely drive their distinct photochemical responses. For Gd^{3+}, one can expect narrow absorption lines between 170–280 nm, due to its $4f$–$4f$ transitions; however, no such transitions were detected in our case due to instrumental limitations. Yb-containing TiO_2 materials are also transparent in visible range of 250–750 nm. The detailed information regarding RE^{3+} energy level structure can be found in the literature [29].

3.3. PL spectroscopy

The light emission spectra of prepared materials under excitation at $\lambda_{exc} = 266$ nm are displayed in Fig. 5. Their photoluminescence excitation spectra at the most intense emission band at about 325 nm (not shown here) exhibit a broad and strong excitation band with a maximum at 365 nm, that coincides very well with the A/B dual-phase TiO_2 absorption band edge (Fig. 3) thus indicating that the band gap of the A/B TiO_2 nanocrystallites makes the main contribution to the RE ions excitation. As shown in Fig. 5, *a*, the emission spectrum of undoped TiO_2 consists of a broad band ranging from ∼350 nm to 800 nm. The emission maximum at 461 nm and the overall width of the signal are likely due to a combination of inter-band and intra-band transitions with those linked to material defects.

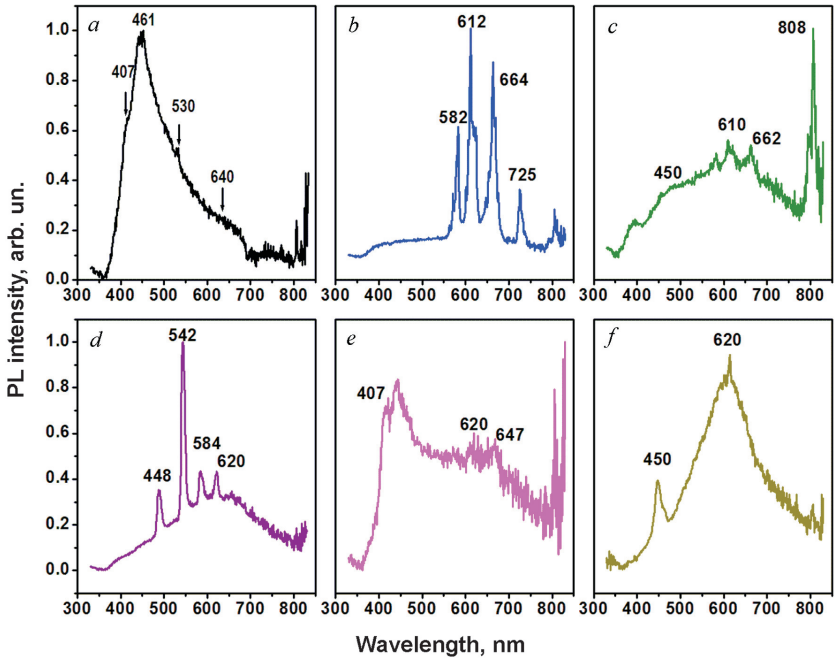

Fig. 5. Normalized room-temperature PL emission spectra of the samples: TiO_2 (*a*), Sm-T (*b*), Tm-T (*c*), Tb-T (*d*), Yb-T (*e*), Gd-T (*f*). The excitation wavelength $\lambda_{exc} = 266$ nm

Sm-T samples clearly exhibit the emission lines originating from Sm^{3+} ions (Fig. 5, *b*). The strongest sharp lines are observed at 582, 612, 664, and 725 nm, which were respectively assigned to $^4G_{5/2} \rightarrow ^6H_{5/2}$, $^4G_{5/2} \rightarrow ^6H_{7/2}$, $^4G_{5/2} \rightarrow ^6H_{11/2}$, and $^4G_{5/2} \rightarrow ^6H_{15/2}$ electronic transitions in Sm^{3+} ions. The PL emission spectrum also clearly shows the multiple splitting of $^4G_{5/2} \rightarrow ^6H_{5/2}$, $^4G_{5/2} \rightarrow ^6H_{7/2}$ and $^4G_{5/2} \rightarrow ^6H_{9/2}$ emission lines due to Stark effect caused by internal crystal fields.

Also, in the measured emission spectra of Tm-T samples (Fig. 5, *c*), emission from Tm^{3+} ions can be recognized with the most intense lines at 610 nm, 662 nm, and 808 nm originating from $^1G_4 \rightarrow ^3F_3$, $^1G_4 \rightarrow ^3F_4$, and $^3H_4 \rightarrow ^3H_6$, transitions in Tm^{3+}, respectively (Fig. 5, *c*). In addition to the sharp emission lines from Tm^{3+}, a broad band centred at about 650 nm is also observed. This broad band can be assigned to the emission from TiO_2 defect centres [30, 31], because the band is also present in the emission spectra of undoped A/B TiO_2 (Fig. 5, *a*). As seen from Fig. 5, *d*, Tb-T material exhibits characteristic Tb^{3+} emission with the most intense emission bands centred at 488 nm, 542 nm, 584 nm, and 620 nm corresponding, respectively, to $^5D_4 \rightarrow ^7F_6$, $^5D_4 \rightarrow ^7F_5$, $^5D_4 \rightarrow ^7F_4$, and $^5D_4 \rightarrow ^7F_3$ electronic transitions in Tb^{3+} ions. Notably, the Yb-T material does not display any expected Yb^{3+} emission signature ($^2F_{5/2} \rightarrow ^2F_{7/2}$) in the 900–1100 nm region [32], potentially due to our NIR detector limitations (Fig. 5, *e*). Instead, a broad UV-vis band is observed, mirroring the profile of undoped dual-phase TiO_2. The notable increase in the emission intensity at ~650 nm is consistent with the presence of oxygen vacancies or other defect states within the TiO_2 band gap [30].

It should be noted that in the crystals, the RE^{3+} electron states are split into the Stark components represented in PL spectra as several narrow lines of the same energy level [33]. However, in our measurements this fine structure was not practically observed (except for the most intensive Sm^{3+} emission, Fig. 5, *b*) indicating that RE^{3+} ions in A/B TiO_2 matrix are probably located in the regions with disordered local environment near the A/B junctions. The emission from RE-doped TiO_2 observed under excitation at a wavelength above the measured A/B TiO_2 band-gap wavelength (266 nm) indicates a nonradiative energy transfer process from titania to the RE^{3+} ions electronic states. The UV light absorbed in the conduction band of A/B TiO_2 is transferred to the emitting states of RE^{3+} ions and the defect states at the A/B junctions and on the particles surface that is further released with photon emission. Due to

developed particles surface and the presence of A/B junctions, a great number of the surface defect states is available for excitation energy transfer to the energy levels of RE^{3+} ions. It worth noting that in our measurements, photoluminescence as a result of energy transfer was observed only from samples doped with Sm^{3+}, Tb^{3+}, and Tm^{3+}, while no emission was observed for Yb^{3+}- and Gd^{3+}-doped TiO_2 materials (Fig. 5, *e, f*). It is also observed from Fig. 5, that Sm-T has a highest emission intensity in comparison with Tb-T and Tm-T materials, a result that confirms the decrease in the energy transfer efficiency in the order $Sm^{3+} > Tb^{3+} > Tm^{3+}$ [10] and suggests the important role of surface defects in the excitation energy transfer process. If these defects states (which can be different in different materials) are located lower by energy than the emitting states of RE ions, no energy transfer to these states could take place, and no RE luminescence can be observed. Therefore, the observation of characteristic luminescence lines of RE^{3+} ions strongly supports their involvement in the electron-hole recombination processes in the RE-doped TiO_2 particles which may be crucial for their photoactivity.

4. Conclusions

The effect of rare earth dopants, Sm^{3+}, Gd^{3+}, Tb^{3+}, Tm^{3+} and Yb^{3+} on optical and luminescent properties of 2%-doped dual phase anatase-brookite (A/B) TiO_2 nanostructures was evaluated, which has not been reported previously. The dual-phase A/B structure of RE-TiO_2 particles used in the study has been confirmed by X-ray phase analysis. The particles had a spherical shape with a typical size of 10–25 μm in diameter being made up of grown together nanocrystallites measuring 5–8 nm. SEM/EDS analysis confirmed successful incorporation of RE-dopants onto the surface of the A/B TiO_2 nanostructure. FTIR spectroscopy revealed the formation of RE–Ti–O and RE–OH bonds near the TiO_2 surface defects. UV-Vis-NIR diffuse reflectance spectra exhibited blue shift of the main absorption band for Gd-T material, also a red shift of the absorption edge was detected for Yb-T. Several characteristic NIR absorption bands were detected for Sm-T, Tm-T and Yb-T materials assigned to $4f$–$4f$ transitions of RE ions, while Gd^{3+}- and Tb^{3+}-doped samples showed no absorption in this region. The estimated E_g band gap energies for A/B TiO_2 doped with Sm^{3+}, Tm^{3+}, Tb^{3+}, Yb^{3+}, and Gd^{3+}ions appeared to be equal respectively to 2.97, 2.93, 2.92, 2.88 and 2.91 eV, compared with $E_g = 3.02$ eV for undoped A/B TiO_2. It was shown that under excitation of RE–TiO_2 particles above the TiO_2 band gap energy, they exhibited characteristic luminescence emission corresponding to $4f$–$4f$ transitions of RE^{3+} ions. It was explained that in RE-doped A/B TiO_2 nanostructures, the regions at A/B junctions or grain boundaries of TiO_2 nanocrystals can easily accommodate RE^{3+} ions and provide for efficient energy transfer from TiO_2 to RE^{3+} ions under appropriate alignment of the excited sates energy levels of the dopant within TiO_2 band gap. Such energy transfer was observed only in samples doped with Sm^{3+}, Tb^{3+}, and Tm^{3+}, while no emission was observed for Yb^{3+}- and Gd^{3+}-doped TiO_2 due to the higher energy of their emission states.

RE-doped A/B dual-phase TiO_2 nanostructures may find potential applications in various optical and engineering fields, such as LEDs, optic systems, and communication devices, as well as heterogeneous photocatalysis.

This work was supported under the Agreement on Scientific Cooperation between the Polish Academy of Sciences and the National Academy of Sciences of Ukraine in the framework of the joint Polish-Ukrainian project "Molecular Dynamics and Optical Properties of Nano-modified Functional Organic Media" for the years 2025–2027, and the SARU Fellowship Program for Researchers at Risk from Ukrainian Universities and the Technical University of Denmark (DTU). TG is highly grateful to Polish Academy of Sciences for the fellowship provided under the Long-Term Program of Support for the Ukrainian researchers at the Polish Academy of Sciences in collaboration with the U.S. National Academy of Sciences.

1. M. Runowski, N. Stopikowska, S. Lis. UV-Vis-NIR absorption spectra of lanthanide oxides and fluorides. *Dalton Trans.* **49**, 2129 (2020).
2. F. Wang, R. Deng, J. Wang, Q. Wang, Y. Han, H. Zhu, X. Chen, X. Liu. Tuning upconversion through energy migration in core–shell nanoparticles. *Nat. Mater.* **10**, 968 (2011).
3. Q. Su, S. Han, X. Xie, H. Zhu, H. Chen, C.-K. Chen, R.-S. Liu, X. Chen, F. Wang, X. Liu. The effect of surface coating on energy migration-mediated upconversion. *J. Am. Chem. Soc.* **134**, 20849 (2012).

4. A.A. Bol, R. van Beek, A. Meijerink. On the incorporation of trivalent rare earth ions in II−VI semiconductor nanocrystals. *Chem. Mater.* **14**, 112 (2002).
5. J. Ming, J. Zhou, X. Liu, F. Zhang. Antenna effect for enhanced near-infrared luminescence in lanthanide-doped nanoparticles: mechanisms, strategies, and applications. *Adv. Mater.* e08521 (2025).
6. H. Maas, A. Currao, G. Calzaferri. Encapsulated lanthanides as luminescent materials. *Angew. Chem. Int. Ed.* **41**, 2495 (2002).
7. D. Yue, W. Lu, L. Jin, C. Li, W. Luo, M. Wang, Z. Wang, J. Hao. Controlled synthesis, asymmetrical transport behavior and luminescence properties of lanthanide doped ZnO mushroom-like 3D hierarchical structures. *Nanoscale* **6**, 13795 (2014).
8. E. Anuja, I. Potheher, M. Meena, M. Vimalan. Impact on bandgap, electrical and magnetic properties of SnO_2 nanoparticles by cerium and samarium. *J. Mol. Struct.* **1320**, 139617 (2024).
9. K.L. Frindell, M.H. Bartl, M.R. Robinson, G.C. Bazan, A. Popitsch, G.D. Stucky. Visible and near-IR luminescence via energy transfer in rare earth doped mesoporous titania thin films with nanocrystalline walls. *J. Solid State Chem.* **172**, 81 (2003).
10. M. Saif, M. Abdel-Mottaleb. Titanium dioxide nanomaterial doped with trivalent lanthanide ions of Tb, Eu and Sm: Preparation, characterization and potential applications. *Inorg. Chim. Acta* **360**, 2863 (2007).
11. Z. Liu, J. Zhang, B. Han, J. Du, T. Mu, Y. Wang, Z. Sun. Solvothermal synthesis of mesoporous Eu_2O_3–TiO_2 composites. *Micropor. Mesopor. Mater.* **81**, 169 (2005).
12. T.A. Khalyavka, V.V. Shymanovska, E.V. Manuilov, N.D. Shcherban, O.Y. Khyzhun, G.V. Korzhak, V.V. Permyakov. The influence of la doping on structural, optical, and photocatalytic properties of TiO_2 in dyes destruction and hydrogen evolution. In: *Nanostructure Surfaces, and Their Applications, Springer Proceedings in Physics, Vol. 246* (Springer, 2021), p. 361.
13. A. Borkowska, J. Domaradzki, D. Kaczmarek. Influence of Eu dopant on optical properties of TiO_2 thin films fabricated by low pressure hot target reactive sputtering. *Opt. Applicat.* **37**, 117 (2007).
14. E. Radha, D. Komaraiah, R. Sayanna, J. Sivakumar. Photoluminescence and photocatalytic activity of rare earth ions doped anatase TiO_2 thin films. *J. Luminesc.* **244**, 118727 (2022).
15. J. Yin, L. Xiang, X. Zhao. Monodisperse spherical mesoporous Eu-doped phosphor particles and the luminescence properties. *Appl. Phys. Lett.* **90**, 113112 (2007).
16. L. Li, C. Tsung, Z. Yang, G.D. Stucky, L.D. Sun, J.F. Wang, C.H. Yan. Rare-earth-doped nanocrystalline titania microspheres emitting luminescence via energy transfer. *Adv. Mater.* **20**, 903 (2008).
17. T. Khalyavka, O. Cabezuelo, N. Shcherban, G. Korzhak, P. Yaremov, R. Burve, E. Coşkun, T.M. Budnyak, J.-C. Grivel. Assessment of rare earth element-doped anatase-brookite composition for photocatalytic hydrogen production and Rhodamine B photodegradation. *J. Alloys Compd.* **1025**, 180292 (2025).
18. T. Khaliavka, N. Shcherban, G. Korzhak, P. Yaremov, I. Kopa, R. Burve, E. Coşkun, J. Grivel. Photocatalytic hydrogen evolution activity of anatase-brookite nanoparticles modified with rare earth metals (Gd, Lu, Tm, Tb, Pr). In: *Proceedings of the 16th International Conference on Nanomaterials – Research & Application, October 16–18, 2024/OREA Congress Hotel Brno, Czech Republic, EU* (2025), p. 88.
19. T. Bezrodna, G. Puchkovska, V. Shymanovska, J. Baran, H. Ratajczak. IR-analysis of H-bonded H_2O on the pure TiO_2 surface. *J. Mol. Struct.* **700**, 175 (2004).
20. R. Bensasson, E.J. Land. Triplet-triplet extinction coefficients via energy transfer. *Trans. Faraday Soc.* **67**, 1904 (1971).
21. E.M. Huseynov, E.A. Huseynova. Infrared spectroscopy of nanocrystalline anatase (TiO_2) particles under the neutron irradiation. *Opt. Mater.* **144**, 114351 (2023).
22. M. Iliev, V. Hadjiev, A. Litvinchuk. Raman and infrared spectra of brookite (TiO_2): Experiment and theory. *Vibr. Spectrosc.* **64**, 148 (2012).
23. Y. Zou, X. Tan, T. Yu, Y. Li, Q. Shang, W. Wang. Synthesis and photocatalytic activity of chrysanthemum-like brookite TiO_2 nanostructures. *Mater. Lett.* **132**, 182 (2014).
24. M. Anpo, M. Takeuchi. The design and development of highly reactive titanium oxide photocatalysts operating under visible light irradiation. *J. Catal.* **216**, 505 (2003).
25. J. Tauc. Optical properties and electronic structure of amorphous Ge and Si. *Mater. Res. Bull.* **3**, 37 (1968).
26. S. K. Sharma, T. Behm, T. Köhler, J. Beyer, R. Gloaguen, J. Heitmann. Library of UV-visible absorption spectra of rare earth orthophosphates, $LnPO_4$ (Ln = La–Lu, except Pm). *Crystals* **10**, 593 (2020).
27. S. K. Sharma, J. Beyer, R. Gloaguen, J. Heitmann. Non-quenching photoluminescence emission up to at least 865 K upon near-UV excitation in a single crystal of orange-red emitting $SmPO_4$. *Phys. Chem. Chem. Phys.* **21**, 25669 (2019).
28. J.A. Capobianco, F. Vetrone, J.C. Boyer, A. Speghini, M. Bettinelli. Enhancement of red emission ($^4F_{9/2} \rightarrow \rightarrow {}^4 I_{15/2}$) via upconversion in bulk and nanocrystalline cubic $Y_2O_3 : Er^{3+}$. *J. Phys. Chem. B* **106**, 1181 (2002).
29. Y. Wang, K. Zheng, S. Song, D. Fan, H. Zhang, X. Liu. Remote manipulation of upconversion luminescence. *Chem. Soc. Rev.* **47**, 6473 (2018).
30. L. Kernazhitsky, V. Shymanovska, T. Gavrilko, V. Naumov, L. Fedorenko, V. Kshnyakin, J. Baran. Photoluminescence of Cr-doped TiO_2 induced by intense UV laser excitation. *J. Lumin.* **166**, 253 (2015).
31. Y. Lei, L.D. Zhang. Fabrication, characterization, and photoluminescence properties of highly ordered TiO_2 nanowire arrays. *J. Mater. Res.* **16**, 1138 (2001).

32. M. Chaika, S. Ubizskii, J. Kajan, T. Gregor, G. Gamazyan, L. Marciniak. On the nature of CT luminescence in Yb^{3+} : YAG single crystal under low photon energy. *Opt. Mater.* **130**, 112548 (2022).
33. A. Szysiak, R. Tomala, H. Węglarz, J. Kajan, M. Słobodzian, M. Chaika. Toward more performant eye safe lasers: Effect of increasing sensitizer amount in Yb^{3+}, Er^{3+} : YAG transparent ceramic on its spectral characteristics. *J. Eur. Ceram. Soc.* **45**, 117365 (2025).

Received 22.12.25

Т. Гаврилко, Т. Халявка, Ж.-К. Грівель, Є. Мануйлов, В. Шимановська, М. Чайка, М. Дрозд

ОПТИЧНІ ТА ФОТОЛЮМІНЕСЦЕНТНІ ВЛАСТИВОСТІ ДВОФАЗНОГО TiO_2 КОМПОЗИТА АНАТАЗ-БРУКІТ, ЛЕГОВАНОГО ІОНАМИ РІДКІСНОЗЕМЕЛЬНИХ ЕЛЕМЕНТІВ

Вперше повідомляється про оптичні й люмінесцентні властивості наноструктурованого двофазного TiO_2 композита анатаз-брукіт (А/Б TiO_2), легованого іонами рідкісноземельних елементів (РЗЕ) Sm^{3+}, Gd^{3+}, Tb^{3+}, Tm^{3+} і Yb^{3+}. Частинки TiO_2, леговані РЗЕ, мали сферичну форму з типовим розміром 10–25 мкм у діаметрі й складалися зі зрощених разом агрегатів нанокристалітів розміром 5–8 нм. SEM/EDS аналіз підтвердив успішне включення легуючих домішок РЗЕ на поверхню частинок TiO_2. За допомогою ІЧ-Фур'є-спектроскопії виявлено утворення зв'язків РЗЕ–Ti–O та РЗЕ–OH поблизу поверхневих дефектних станів. Спектри дифузного відбиття в ультрафіолетовому (UV), видимому (Vis) і ближньому інфрачервоному (NIR) діапазонах показали короткохвильове зміщення максимуму основної смуги поглинання TiO_2 для легуючої домішки Gd^{3+} та довгохвильове зміщення краю поглинання для Yb^{3+}. Кілька характерних смуг поглинання іонів РЗЕ також виявлено для зразків TiO_2, легованих Sm^{3+}, Tm^{3+} і Yb^{3+}, що відповідають їх переходам $4f$–$4f$, тоді як зразки, леговані Gd^{3+} та Tb^{3+}, не показують поглинання в цій області. Розраховані енергії забороненої зони TiO_2, легованого РЗЕ, становили E_g = 3,02 еВ для нелегованих зразків і E_g = 2,97, 2,93, 2,92, 2,88 та 2,91 еВ для зразків, легованих Sm^{3+}, Tm^{3+}, Tb^{3+}, Yb^{3+} і Gd^{3+}, відповідно. Показано, що під час збудження нанокристалів А/Б TiO_2 вище енергії забороненої зони TiO_2 частинки демонструють характерну люмінесценцію, яка відповідає переходам $4f$–$4f$ іонів $РЗЕ^{3+}$. Пояснено, що в двофазних наноструктурах А/Б TiO_2, легованих РЗЕ, області інтерфейсу А/Б або поверхні поділу зерен у нанокристалах TiO_2 можуть легко вміщувати іони $РЗЕ^{3+}$ і забезпечити ефективну передачу енергії від TiO_2 до іонів $РЗЕ^{3+}$ за умови відповідного розташування збуджених енергетичних рівнів легуючої домішки в забороненій зоні TiO_2. Таке перенесення енергії спостерігалося лише у зразках, легованих Sm^{3+}, Tb^{3+} і Tm^{3+}, тоді як для TiO_2, легованого Yb^{3+} і Gd^{3+}, випромінювання не спостерігалося через вищу енергію їхніх збуджених станів. Двофазні наноструктури А/Б TiO_2, леговані РЗЕ, можуть мати застосування в багатьох оптичних й інженерних пристроях у різних галузях техніки, таких як світлодіоди, оптичні та комунікаційні пристрої, а також у гетерогенному фотокаталізі.

Ключові слова: TiO_2, нанокристали, рідкісноземельні елементи, поглинання в UV-Vis-NIR діапазоні, люмінесценція, перенесення енергії.